DOI: 10.1021/ma101777d

Macromolecules
ARTICLE

Molecular Dynamics of Reversible and Irreversible Melting in Chain-Folded Crystals of Short Polyethylene-like Polymer

Takashi Yamamoto*

Department of Physics and Informatics, Yamaguchi University, Yamaguchi 753-8512, Japan

Received August 4, 2010; Revised Manuscript Received October 10, 2010

ABSTRACT: Crystallization and melting are fundamental thermal processes in crystalline polymers. In contrast to recent considerable efforts to simulate molecular processes of crystallization, investigations of melting in polymer crystals are still rare. The present report deals with molecular dynamics modeling of melting in chain-folded lamellae of short polyethylene-like molecules made of 100 methylene units. We observe two types of melting with distinct molecular mechanisms: equilibrium melting at the fold surface and nonequilibrium melting at the growth front. The former fold-surface melting is very quick and reversible, giving increasingly thinner lamellae at higher temperatures. Large molecular mobility in the crystal is suggested to be the essential prerequisite for this specific mode of melting. The latter type of melting at the growth front is much slower and irreversible, and it becomes apparent right after the end of rapid surface melting. It is found that the rate of the irreversible melting shows intriguing similarity to the supercooling dependence of the crystallization rate. Large dynamic heterogeneity in the chain-folded crystals is also found, the molecular mechanism of which is closely correlated to the chain conformation at the fold surface. The presence and specific time dependence of solid-state diffusion between different phases (crystalline phase, amorphous phase at the fold surfaces, and isotropic melt phase) are also discussed.

1. Introduction

Many polymeric materials, whether synthetic or natural, are crystalline. They consist of chain-folded lamellar crystals and intervening amorphous regions. Since mesoscopic and macroscopic structures of the polymeric materials dominate many of their physical properties, the molecular mechanism of polymer crystallization has been one of the central issues in macromolecular science.[1−4] Molecular dynamics of long intertwined chains building up neat chain-folded crystals have given researchers many inspirations, but they are quite complex and pose great obstacles for experimental investigations.[5−7]

Polymer molecules usually crystallize from highly supercooled melts or solutions, thereby giving mesoscopic structures not fully equilibrated in thermodynamic sense. The polymer crystals often show unusual thermal behavior; they melt at much lower temperatures than equilibrium melting points, and melting and crystallization often go together, making their clear separations very difficult.[1,8,9] Though melting of polymer crystals has not so far attracted as much attention as crystallization, renewed interest is recently shown in the melting owing to the advent of new experimental techniques in thermal analysis, NMR, X-ray diffraction, etc., and also to the necessity of deeper understanding of annealing and recrystallization processes.[10−15]

Computer simulation studies, with various molecular models of different fidelity, have been reported to clear up unsolved mysteries in polymer crystallization.[8,9,16−27] However, molecular level investigations of melting in chain-folded crystals are still rare.[28] We here attempt a molecular dynamics (MD) simulation of melting in a simple polyethylene-like polymer. We will show the presence of two kinds of melting: fast reversible melting at the fold surface and slower irreversible melting at the growth front. We will also find that the molecular mechanisms of the surface melting are closely related to large molecular mobility in the crystalline phase and that there exists peculiar heterogeneity in dynamical properties of crystalline chains.

*E-mail: yamamoto@mms.sci.yamaguchi-u.ac.jp.

2. Simulation Method

2.1. Model and Method. In this paper, we focus on universal features in crystallization and melting of a simple model polymer. Complex chemical structures and conformations such as those in helical polymers pose specific problems, but they are separate subjects of research.[29,30] We here consider a polyethylene (PE)-like polymer, for which crystallization has been studied in our earlier papers.[9,22,23] Our polymer molecules are rather short, being composed of 100 beads; studies on much longer polymers are undoubtedly very important, and they are themes of our future investigations. The beads are considered to have molecular mass 14 representing the methylene units, and they are connected by harmonic springs with a potential energy of the form

$$U_{\mathrm{b}}(r) = k_{\mathrm{B}}(r - r_0)^2/2 \tag{1}$$

and each pair of beads more than two bonds apart interact via van der Waals forces of the Lennard-Jones type

$$U_{\mathrm{vdW}}(r) = 4\varepsilon\left[\left(\frac{\sigma}{r}\right)^{12} - \left(\frac{\sigma}{r}\right)^{6}\right] \tag{2}$$

,where the interactions are cut off at $r = 2.0\sigma$. The molecules are semiflexible, the flexibility of which is adjusted to reproduce the characteristic ratio of real polyethylene, by adding the potential for bond angle bending

$$V_{\mathrm{bent}}(\theta) = a - b(\cos\theta - \cos\theta_0) + d(\cos\theta - \cos\theta_0)^3 \tag{3}$$

where θ is the C−C−C bond angle and $\theta_0 = 108.78°$; the potential (3) is devised to give the lowest energy of 0 kcal at $\theta = 180°$,

 Published on Web 10/22/2010

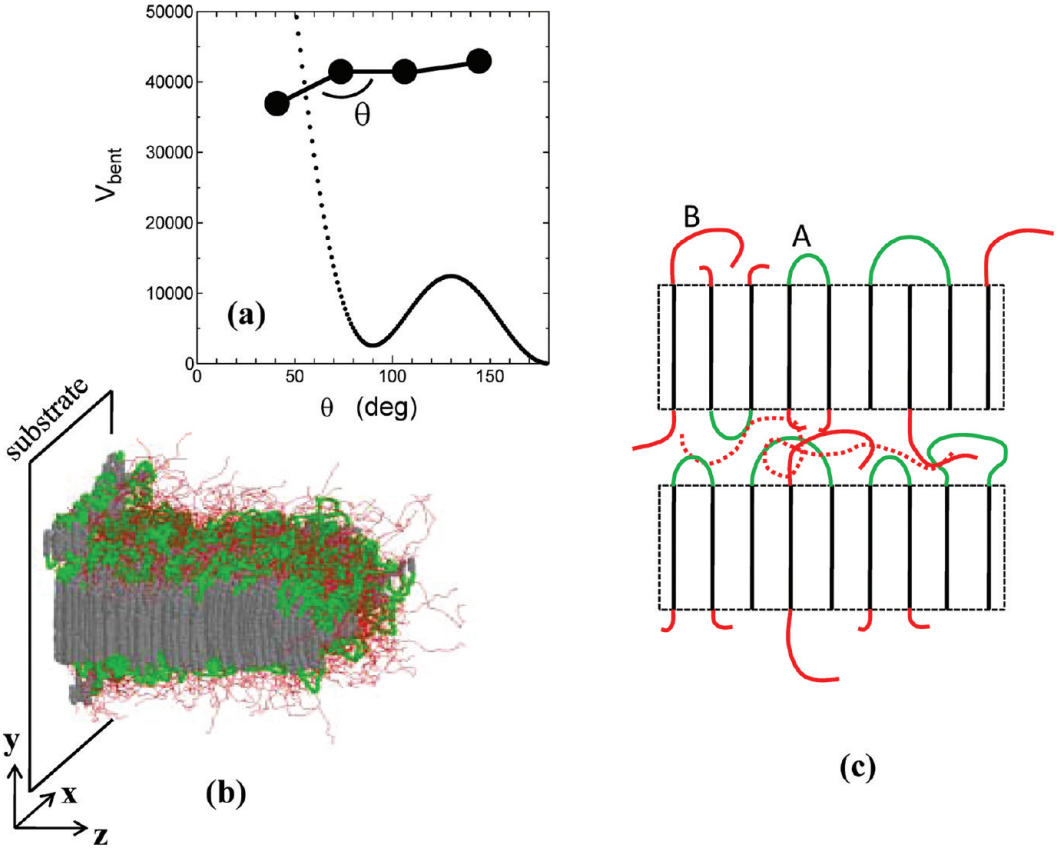

Figure 1. (a) Potential form of the bending energy V_{bent} representing the stiffness of our model polymer. (b) Chain-folded lamella growing from the left substrate. The lamella grows along the z-axis, and the direction of crystalline chains is along the y-axis. (c) A schematic image of the amorphous phase chains; once-folded chains (A), "half-crystallized" chains with long cilia (B), and chains floating within the interface (red dotted line). In both figures, crystalline stems are depicted in gray, folds in green, and cilia in red.

Table 1. List of Parameters and Their Values

parameter	values	units
m	14×10^{-3}	kg/mol
k_b	3.5×10^{25}	J/(m^2 mol)
r_0	0.154	nm
a	7.440×10^3	J/mol
b	2.297×10^4	J/mol
d	7.386×10^4	J/mol
θ_0	108.78	deg
ε	598.64	J/mol
σ^a	0.392	nm

[a] σ is a unit length in reduced unit.

the local minimum of 2.51 kJ/mol at $\theta = 90°$ (90° kink), and the energy barrier of about 12.54 kJ/mol at $\theta = 130°$ (Figure 1a). All the values of relevant parameters are listed in Table 1, and they were found to reproduce various physical properties of short polyethylene such as the heat of fusion $\Delta H = 0.97$ kcal/mol of atoms, the melting point T_m around 380 K, the characteristic ratio $\alpha = 7.8$, and also the center-of-mass diffusion coefficient $D_G = 1.34 \times 10^{-6}$ cm^2/s in the melt at 370 K.[23]

We place 1280 chains within the MD cell of a given size $L_x = 30\sigma$, $L_y = 30\sigma$, and $L_z = 70\sigma$, where the volume of the MD cell is taken slightly larger than that of fully melted state in order to reserve an empty space on the right side of the cell, thereby keeping zero pressure condition. By use of periodic boundary conditions in the x- and y-axis directions, we consider a film of thickness 70σ extending infinitely over the substrate (Figure 1b). In order to provide nucleation sites for the growth of large single crystals of a given orientation, we consider, as in our previous papers,[9,22,23] a solid substrate which exerts strong attraction for the chains, where the substrate−polymer interactions are calculated by use of a method proposed by Steele.[31] Present simulations are conducted with a conventional NVT ensemble by use of the leapfrog method, with a time step of 3.2 fs, and the temperature is controlled by the velocity scaling every 30 steps. Throughout the paper, the unit length is taken as the van der Waals parameter σ.

2.2. Static and Dynamic Order Parameters. First, we must identify crystalline domains in the system. As in our previous studies,[9,22,23] we consider that the crystal domains are made of well-aligned and closely packed C−C bonds. We pick up all C−C bonds that are nearly parallel to the y-axis with angles less than 20°. Out of these candidate C−C bonds we consider those having at least three neighbors as crystalline bonds; the two bonds are considered neighboring when the vector $\mathbf{r} = (r_x, r_y, r_z)$ connecting the centers of the bonds satisfies the following relations: $0.7\sigma < (r_x^2 + r_z^2)^{1/2} < 1.3\sigma$ and $|r_y| < r_0/2$. Then the crystallinity χ_c, the fraction of atoms within the crystal domains, is the simplest measure of crystallization and melting.

Besides the crystalline atoms described above and the chains floating in the noncrystalline regions, we must find atoms forming chain folds and cilia (Figure1c); the former are connecting crystalline stems of the same lamella, while the latter are segments with free chain ends. We have also atoms forming crystal defects (kinked bonds), whose C−C bond directions deviate from the y-axis more than 20°. In most of the present discussions, except estimating the χ_c, defect atoms (bonds) are included in the crystalline component, since they are parts of the crystalline phase from the structural point of view.

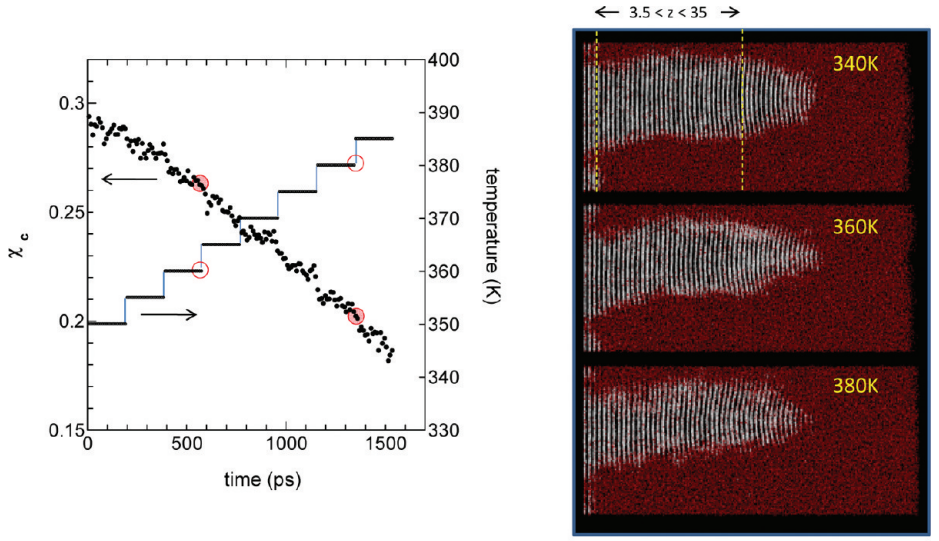

Figure 2. (a) Decrease in crystallinity χ_c during fast stepwise heating 5 K/198 ps. (b) Snapshots of surface-melting lamellae during the heating run: initial lamellae at 340 K and at 360 and 380 K (red circles in (a)). The snapshots are viewed along the *x*-axis, where white lines represent crystalline stems of the chain-folded lamellae and red background is the melt phase.

A typical dynamical property of chains in the melt is center-of-mass diffusion coefficient D_G, which we estimated to be 1.34×10^{-6} cm^2/s at 370 K from the squared displacements within several tens of nanoseconds.[23] In the present study of mobility in crystals, however, the chains are restricted to move along the folded contours, and D_G is not always a suitable variable to describe chain diffusion in crystals. We here consider a short-term mobility in terms of average displacement of atoms within τ of about a hundred picoseconds, $\mu_n(\tau) = \langle (r_n(t) - r_n(t+\tau))^2 \rangle^{0.5}$, and the distribution $P(\mu)\,d\mu$ representing the number of atoms whose mobility μ_n satisfies $\mu < \mu_n < \mu + d\mu$.

3. Results of Simulations

3.1. Melting of Chain-Folded Lamellae. Our previous simulations showed that the crystal growth of chain-folded lamellae virtually halts around 380 K, and the temperature was regarded as the approximate melting point T_m or more precisely the melting point of once-folded lamellae as will be discussed later. When the lamellae grown at lower temperatures are brought close to T_m, they show appreciable melting. Melting at the fold surface takes place even at temperatures far below T_m. At temperatures around T_m or above T_m, the lamellae also show usual melting with retreating growth front. We here investigate these two types of melting separately and find that they have different characteristic times and distinct molecular mechanisms.

3.1.1. Reversible Melting at the Fold Surface. Well-developed lamellae crystallized at 340 K were heated rapidly up to 385 K by a stepwise increase of temperature (5 K/196 ps). Figure 2a shows that the crystallinity χ_c decreases continuously from 0.29 to 0.18. However, the lamellae did not show expected retreat of the growth front (Figure 2b); the rapid melting must be taking place at the fold surface.

To confirm the surface melting, we calculated profiles of the lamella thickness. In order to reduce statistical errors, the lamella thickness $l(x, z)$ at given position (x, z) was estimated from the numbers of crystalline atoms (including crystal-defect atoms) within the rod region along the *y*-axis of volume $2\sigma \times 2\sigma \times L_y$. The region includes ~3.7 crystalline stems, and the thickness given in Figure 3 is about 3.7 times the real

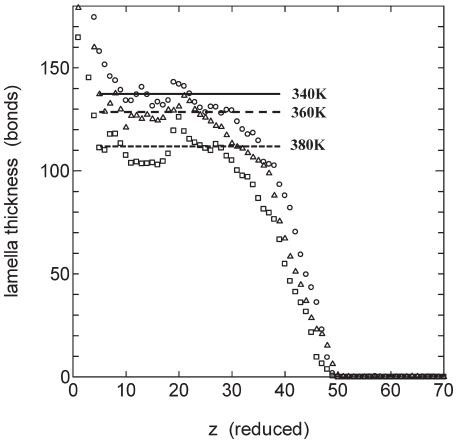

Figure 3. Changes in the lamella thickness profile with heating: initial lamella at 340 K (○), t = 198 ps at 360 K (Δ), and t = 198 ps at 380 K (□). The abscissa z is the distance from the substrate, and the lamella thickness was estimated from the number of crystalline bonds (including defects) within the rod regions of width $(2\sigma)^2$ along the chain axis, thereby giving about 3.7 times the real stem length. The horizontal lines are only approximate measures of average thickness of the lamellae.

lamella thickness; the thickness $l(x, z)$ was further averaged over x to give a depth profile $l(z)$ vs z from the substrate (Figure 3). We can notice considerable lamellar thinning of about 18% by the temperature increase from 340 to 380 K; the lamella thinning of about 18% might seem to be inconsistent with the corresponding decrease in χ_c of about 30% (Figure 2a), but this is due to the fact that in estimating the lamella thickness we included defect atoms as members of the crystalline stems.

Melting at the fold surface has been studied in various synthetic polymers, such as polyethylene, poly(ethylene oxide), etc.[10,11,14,15] It is now well-established that the surface melting is reversible and occurs at temperatures well below T_m[14] and that the surface melting is fast enough to follow rapid temperature modulation of 1 °C/60 s at least.[11] Simple thermodynamic arguments were also proposed to explain how the boundary between the crystal core and the fold surface moves.[14,15] By use of modulated temperature DSC, Hu et al. recently proposed an interesting molecular model of surface melting and maintained

that active chain diffusion within the crystalline phase (or the presence of crystalline dispersion) is an essential prerequisite for the surface melting.[10]

Though the time scales of experiments are quite different from our MD simulation, we here test the reversibility of the surface melting by heating and cooling runs of 5 K/196 ps. As will be explained in the next section, the characteristic time of the surface melting in our present system is of order of 500 ps. By the temperature jump every 200 ps, we expect that the lamella follows approximate equilibrium conditions. Figure 4 shows the changes in χ_c during the heating and cooling runs. By a small temperature cycle $\Delta T = 10$ K, from 350 K (a) to 360 K (b) and back to 350 K (a′), the crystallinity decrease of about 3% is nearly recovered. The decrease in crystallinity of about 3% within 10 K gives excess heat capacity $C_p = \Delta H\, d\chi_c/dT$[10] of about 0.84 J g^{-1} K^{-1}, where the heat of fusion ΔH is around 280 J g^{-1} from experiments and simulation.[10,23] Correspondence with a recent experimental C_p of about 0.6 J g^{-1} K^{-1} is rather surprising, taking much smaller crystallinity of our system compared with those of experiments. When the temperature is raised up to 380 K (c), on the other hand, irreversible melting is considered to make large contributions, and the recovery of χ_c (a″) is only partial.

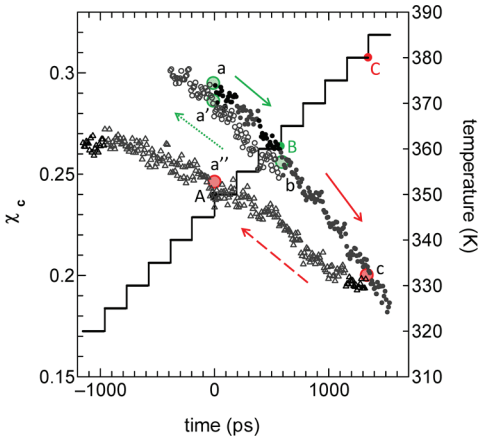

Figure 4. Changes in the crystallinity χ_c during heating (●) and cooling from 360 K (B) (○) to 340 K (A) and from 380 K (C) to 320 K (△). Both the heating and cooling rates are 5 K/198 ps. By the small temperature cycle (ABA), the crystallinity nearly recovers (a b a′), while by the larger temperature cycle (ACA) the crystallinity does not fully recover at least by the present fast heating and cooling.

The molecular mechanism of the surface melting/recrystallization is of considerable interest. A simple picture is to consider it to be a simple breathing mode where the melting at the fold surface gives longer folds and cilia while recrystallization is a simple reverse process back to the original compact forms. If such a simple melting/recrystallization would take place at the fold surface, we could expect parallel increase/decrease in the fractions of folds and cilia atoms with decreasing/increasing crystallinity. We here examine the changes in the amount of cilia and folds during the surface melting. In order to avoid complexity due to contributions from wedged growth front, we consider a region $3.5\sigma < z < 35\sigma$ where the lamella has nearly constant thickness (Figures 2b and 3). During the progress of surface melting, decrease in the number of crystalline core atoms ΔN_{core} causes the increase in the number of cilium atoms ΔN_{cilia}, fold atoms ΔN_{folds}, and atoms forming crystal defects $\Delta N_{defects}$:

$$\Delta N_{core} + \Delta N_{cilia} + \Delta N_{folds} + \Delta N_{defects} = 0 \qquad (4)$$

Considering that crystalline atoms are sum of core atoms and defect atoms, $N_{cryst} = N_{core} + N_{defects}$, we here define the fractions of crystalline, fold, and cilia atoms, χ'_c, χ'_{folds}, χ'_{cilia}, within the region $3.5 < z < 35$ as the ratios $\chi'_c = N_{cryst}/N_{all}$, $\chi'_{cilia} = N_{cilia}/N_{all}$, $\chi'_{folds} = N_{folds}/N_{all}$, where $N_{all} = 63\,564$ is the total number of atoms within the region. Then, from eq 5, the changes in χ'_c, χ'_{folds}, χ'_{cilia} satisfy the relation $\Delta\chi'_c + \Delta\chi'_{cilia} + \Delta\chi'_{folds} = 0$. Figure 5 shows the changes $\Delta\chi'_c = \chi'_c(T) - \chi'_c(T_0)$, $\Delta\chi'_{folds} = \chi'_{folds}(T) - \chi'_{folds}(T_0)$, $\Delta\chi'_{cilia} = \chi'_{cilia}(T) - \chi'_{cilia}(T_0)$ vs T during (a) the rapid heating ($T_0 = 340$ K) and (b) the rapid cooling ($T_0 = 360$ K). By heating from 340 to 370 K, the decrease in χ'_c of about 0.05 is compensated by the increases in χ'_{folds} and χ'_{cilia} of about 0.01 and 0.04, respectively (Figure 5a). Contrary to the simple breathing mode of the surface melting, the elongation of folds is unexpectedly smaller than that of cilia; the fold loops loosened by the surface melting are suggested to be tightened up by the transfer of atoms from folds to cilia through sliding diffusion of chains.

To estimate the degree of chain transport quantitatively, we show in Table 2 the changes with temperature in various relevant quantities. We can assume that the total number of atoms N_{all} within the region $3.5\sigma < z < 35\sigma$ is nearly constant, while N_{cilia}, N_{folds}, and N_{cryst} vary with progress of surface melting. The total number of atoms N_{sum} is the sum

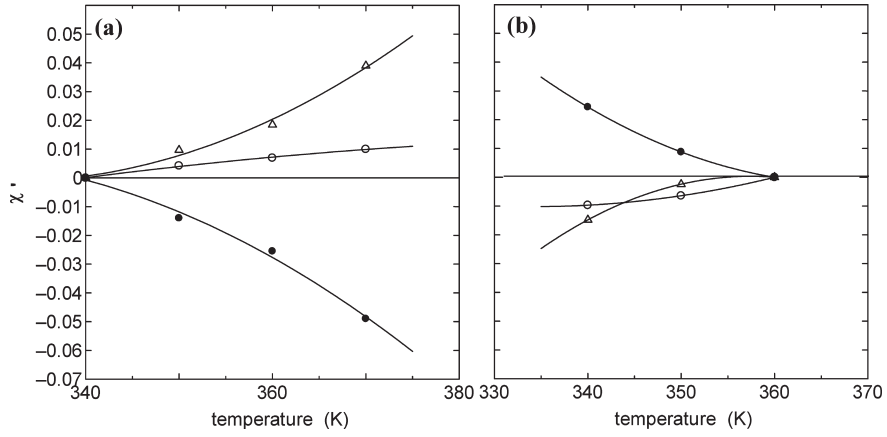

Figure 5. Changes in the fraction of crystalline (plus defect) bonds χ_c' (●), fold bonds χ'_{folds}(○), and cilia bonds χ'_{cilia} (△) (a) during stepwise heating from 340 to 370 K and (b) during cooling from 360 K back to 340 K. Fractions χ' are here defined as the number of crystalline, cilia, and fold atoms within the region $3.5 < z < 35$ divided by the total number of atoms (62 564) within this region; the lines are fitted by the least-squares method with second-order polynomials. The folds loosened by the surface melting are suggested to be tightened through chain transfer to cilia.

Table 2. Characteristic Values of Parameters vs Temperature

parameter	unit	340 K	350 K	360 K	370 K
N_{all}	atoms	62564	62564	62564	62564
N_{cilia}	atoms	14395	15002	15553	16836
N_{folds}	atoms	4836	5102	5271	5461
N_{cryst}	atoms	33268	32395	31675	30202
N_{sum}	atoms	52499	52499	52499	52499
N_{chain}	chains	525	525	525	525
χ'_c		0.53	0.52	0.51	0.48
$N_{type\ A}$	chains	359	359	359	359
$N_{type\ B}$	chains	166	166	166	166
$N_{cilia\text{-}seg}$	segments	1050	1050	1050	1050
N_{stems}	segments	884	884	884	884
L_{cilia}	bonds	13.7	14.3	14.8	16.0
L_{folds}	bonds	13.5	14.2	14.7	15.2
L_{stems}	bonds	37.6	36.6	35.8	34.2

of N_{cilia}, N_{folds}, and N_{cryst}, which shows us the number of relevant chains N_{chains} that constitute the growing lamella. The number of type A chains, that is, the number of folds, was counted directly to be $N_{type\ A} = 359$, which we can be safely assumed to be constant within the present temperature cycle. Then the number of type B chains is given by $N_{type\ B} = N_{chains} - N_{type\ A} = 166$. Since each chain has two chain ends, the total number of cilia segments $N_{cilia\text{-}seg}$ is given as $2N_{chains} = 1050$. The number of crystalline stems is also estimated as $N_{stems} = 2N_{type\ A} + N_{type\ B} = 884$. Using these values, the average lengths of cilia, folds, and stems are given by $L_{cilia} = N_{cilia}/N_{cilia\text{-}seg}$, $L_{folds} = N_{folds}/N_{type\ A}$, and $L_{stem} = N_{cryst}/N_{stems}$ (Table 2).

The average lamella thickness L_{stem} (340 K) is about 37.6 bonds, which corresponds to the thickness given in Figure 3. The decrease in χ'_c from 0.53 (340 K) to 0.48 (370 K) suggests the decrease in the lamella thickness to $37.6 \cdot (0.48/0.53) = 34.1$ bonds, and indeed the estimated L_{stem} is 34.2 bonds (Table 2). The shortening of stems by 3.4 bonds is considered to be distributed to folds and cilia by the total ratio 1:4 (Figure 5a); this comes from the changes in the total numbers of atoms for cilia and folds, N_{cilia} and N_{folds} (Table 2). Though the numbers of cilium and fold segments are not equal, a detailed estimation in Table 2 shows that the average cilia length L_{cilia} increases by 2.3 bonds, while the fold length L_{folds} increases only by 1.7 bonds. Since the fold has two legs, each leg of the fold increases only 0.85 bonds in length. It is thus considered that the decrease in the crystalline stem length of about 3.4 bonds is roughly redistributed 2.3 bonds to cilia and 0.85 bonds to folds, though with small numerical errors. Equipartition of the melted crystalline bonds to folds and cilia would give elongation of about 1.7 bonds for both, but the present estimation shows that about half of the loosened folds are transferred to cilia.

During cooling from 360 K back to 340 K, on the other hand, the crystallinity lost during heating is almost recovered. However, the shrink in the folds and cilia does not follow exactly the reverse path (Figure 5b); faster tightening of folds and slower shortening of cilia may be reasonable when we consider that the former needs only slight adjustments of chains while the latter requires long-range chain transfer back to the original positions.

The elongation of cilia at the expense of tightening of folds is entropically favorable, and in addition the presence of longer folds would be geometrically unfavorable due to overcrowding at the fold surface. These may provide good reasons for the complicated molecular processes observed during the surface melting. Sliding diffusion of our short chains is much easier than in longer chains, which could make the chain transfer very pronounced. In systems of longer polyethylene, chains are folding many times, and the tightening up of loose folds must be accomplished by chain transfer to other folds, not necessarily to cilia. In any case, active chain diffusion within the crystal will be a prerequisite for such mechanism to be operative in the surface melting.[10]

3.1.2. Irreversible Melting at the Growth Front. When the chain-folded lamellae crystallized at lower temperatures are jumped to temperatures around or above T_m, the rapid surface melting first takes place which is then followed by slower irreversible melting. Figure 6a shows the melting after the temperature jump from 370 K to various higher temperatures. Within the initial 1 ns after the temperature jump, the crystallinity rapidly decreases due to the surface melting, while the slower melting that follows represents usual melting of lamellae where the growth front withdraws, keeping the wedge shape (Figure 6b).

The melting process is separated by assuming two distinct contributions: $\chi_c = \chi_{fast} + \chi_{slow}$. The fast process can be fitted by an exponential form, $\chi_{fast}(t) = \chi_{fast\_0} \exp(-t/\tau_s)$, while the slower melting is well represented by a linear decrease. Typical time evolutions of the former term $\chi_{fast}(t)$ are plotted in log scale vs time in the inset of Figure 6a, which shows that the typical time constant of the fast melting is around 500 ps at both 380 and 400 K, more precisely within the range between 370 and 400 K. The time constant of 0.5 ns in polymer crystallization is considered surprisingly small, though experimental information to be compared is at present very scarce. The crystalline lamellae we obtained by the simulation may be considered, as will be discussed in the last section, metastable crystalline states.

Fold surfaces of the metastable lamellae could melt and recrystallize within such a short time. However, it can also be a reflection of our molecular model. Our molecular model was originally so devised that it shows accelerated crystallization, where we neglected the torsion angle potential and made the straight chain conformation the most stable one.

Above 370 K, the processes of slow melting are rather simple (Figure 6a). Figure 7 shows the rate of slow melting (negative $d\chi_c/dt$) vs temperature together with the crystallization rate (positive $d\chi_c/dt$) taken from our previous papers.[23] However, melting at lower temperatures is a little bit complicated (see inset of Figure 7). At 360 K, the lamellar crystal shows initial melting with decreasing crystallinity up to 10 ns, but it soon resumes recrystallization. The melting rate at 360 K (Figure 7) is thus estimated from the initial slope within 10 ns; it is also found that the recrystallization rate after 10 ns is very close to that observed in our previous work.[23]

As shown in Figure 7, the slow melting becomes noticeable around 360 K and is much accelerated above the "equilibrium" melting point 380 K. As described before, higher temperatures give increasing thinner lamellae due to the surface melting. Subsequent slow melting is therefore the melting of these thinned lamellae. Increasingly thinner lamellae at higher temperatures could cause increasingly faster melting kinetics of Figure 7.

We here estimate the velocity of the retreating growth front. We have confirmed that the slowly melting lamellae keep constant thickness, and therefore the velocity of the growth front position $z_{GF}(t)$ satisfies the relation $z_{GF}(t)/z_{GF}(0) \cong \chi_c(t)/\chi_c(0)$. Since $z_{GF}(0)$ is around 40σ (Figure 6b, for example) and χ_c and $\chi_c(0)$ are known from Figures 6 and 7 to be about 2.4×10^{-3} ns^{-1} (3.5×10^{-3} ns^{-1}) and 0.23 (0.16), respectively, at 370 K (390 K), the velocity of the retreating growth front is estimated to be around 0.16 nm/ns (0.32 nm/ns). Compared with the velocity of the lamella thinning by the surface melting, about 0.5 nm (3.4 bonds) retreat (Table 2) within the characteristic time of about 0.5 ns, the velocity of the growth front retreat is slightly smaller. Much slower decreases in χ_c for the

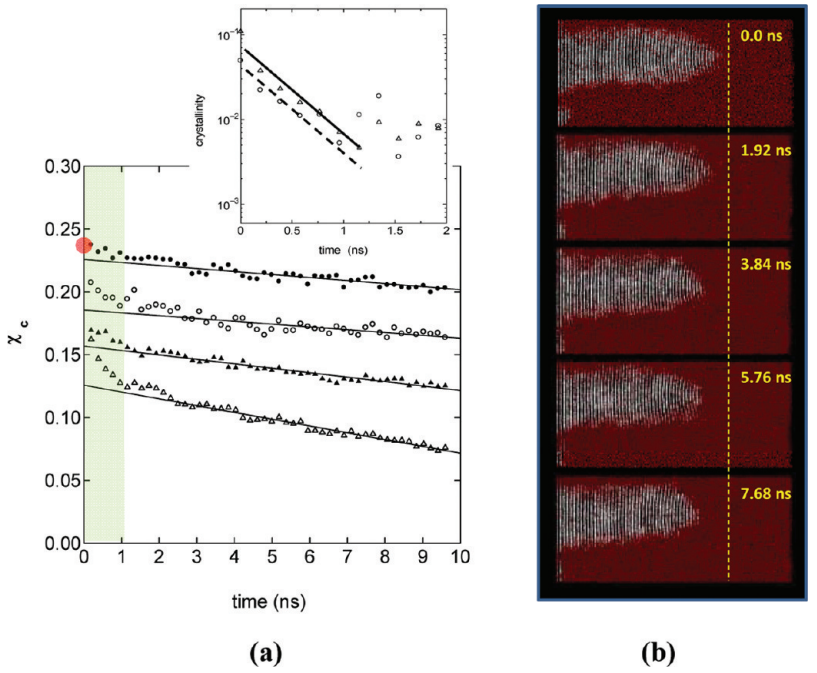

Figure 6. (a) Melting of the lamellae, initially grown at 340 K, at 370 K (●), at 380 K (○), at 390 K (▲), and at 400 K (△). After rapid initial decreases in the crystallinity (χ_{fast}) within about 1 ns due to the surface melting, there follow gradual decreases (χ_{slow}) that represent usual melting of lamellae. Solid lines are fitted by the least-squares method. Initial changes in χ_{fast} are plotted in log scale (inset), which clearly show exponential decreases. (b) Snapshots of gradually melting lamella vs time at 370 K. The growth front is appreciably retreating with time. A vertical yellow line is for the ease of identifying withdrawal of the growth font.

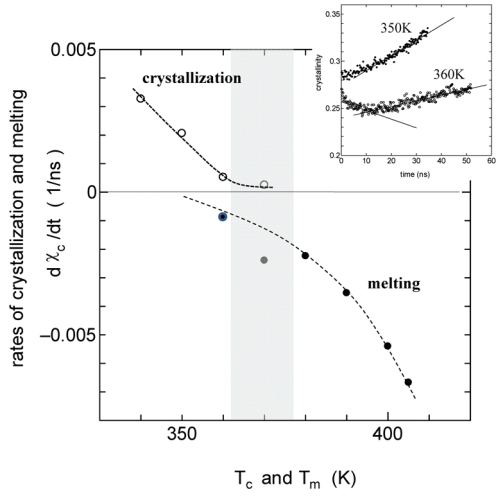

Figure 7. Rate of slow melting vs temperature (●), together with the crystallization rate (○) taken from our previous work.[23] Shown in the inset are the changes in χ_c with time after temperature jumps from 340 to 350 K (●) and to 360 K (○); transient melting is clearly observed at 360 K, which is followed by recrystallization. The melting rate at 360 K was estimated from this initial transient melting, while the rate of regrowth after 10 ns showed good correspondence with our previous simulations of crystal growth directly from the substrate.[23]

growth front melting (Figure 6) is considered largely due to the fact that the growth front melting is a "one-dimensional" melting of thin lamellae, while the surface melting takes place at the wide "two-dimensional" surface of the lamellae.

It is also suggestive that the melting rate and its temperature dependence are similar to those of crystallization (Figure 7). At present, we have no definite idea as to the origins of such similarity, but some authors suggested the presence of free-energy barrier in the melting process.[12] Hu et al. also reported in their lattice Monte Carlo simulation a similar continuity in the melting and crystallization rates vs temperature for the integer-folded lamellae. They also observed transient melting of folded-chain crystal which was followed by recrystallization into extended form. Unfortunately, we could not observe crystallization into chain-extended form even at temperatures close to the melting point; we suspect crystallization of our polymer into the extended chain form is too slow to be observed by direct MD simulation.

Molecular trajectory of melting at the growth front is also very intriguing. When the growth front retreats, the crystalline stem becomes shorter at the wedged growth front. The shortening of the stems is accompanied by increased disordering of tails or cilia. The chains at the growth front gradually lose conformational order and finally detach from the crystal surface merging into the melt (Figure 8).

3.2. Heterogeneous Mobility in the Crystal and Structure of the Fold Surface. Polymer crystals are usually conceived to be ordered homogeneous objects with much lower molecular mobility than in amorphous phases. However, many of the amorphous segments (folds and cilia) are chemically linked to the crystalline stems, and they are forced to move more or less cooperatively with crystalline stems. The apparently conflicting images about the chain mobility in such interconnected systems are not always well understood.

As described above, our present simulation of surface melting suggested the importance of chain diffusion within the crystals. Recent experiments by NMR have verified active segment exchanges between crystalline and amorphous regions revealing very dynamic aspects in crystalline polymers.[32−36] Recent computer simulation studies also suggested that large molecular mobility in crystalline regions plays a very important role in the development and perfection of the crystalline order[37] and also in reorganization or lamella thickening.[9,38]

Our present concern in this section is the correlation between chain mobility in crystal and conformation of chains at the fold surface. We here study lamellae at 340 and 360 K; the former lamellae are still growing, while the latter lamellae grow very

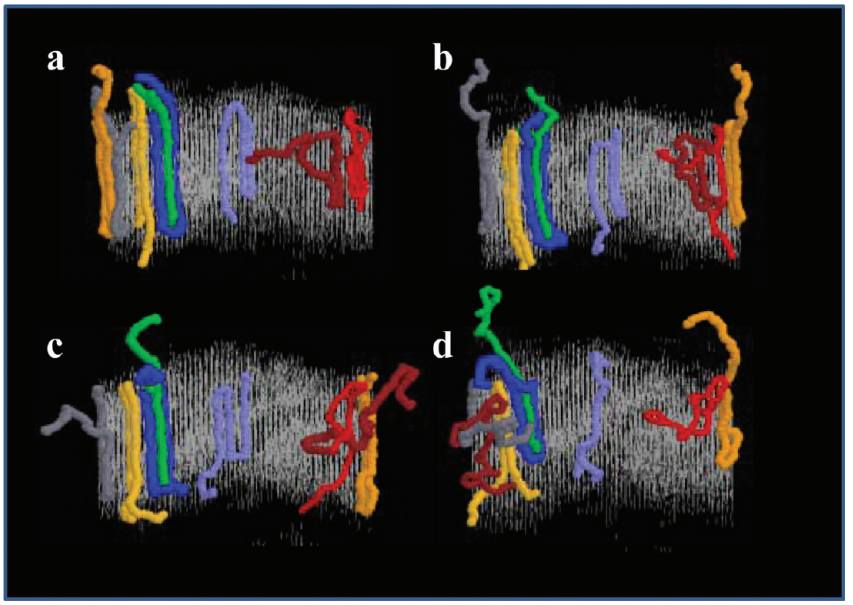

Figure 8. Trajectories of eight chains near the growth front of lamella which is melting at 370 K: (a) at $t = 1.92$ ns, (b) at $t = 3.84$ ns, (c) at $t = 5.76$ ns, and (d) at $t = 9.6$ ns.

slowly and are nearly standing still (Figure 7). As a measure of chain mobility in the melt, center-of-mass diffusion coefficient D_G or time constant of overall relaxation $\tau_{rot} \approx R_n^2/D_G$ has been used; in our present model D_G was estimated to be about 1.3×10^{-6} cm^2/s,[23] and the resulting τ_{rot} of order of 200 ns was much longer than the time scale of our MD simulation. In the present study of crystals, chains are strongly constrained to move along their folded contours. In addition, many segments change their positions from the crystalline region to the melt and vice versa; polymer segments do not always spend a long time within a single phase, long enough to define usual diffusion coefficient. As a measure of chain mobility in crystals, we therefore consider average displacement of each atom within a given short interval of time τ, $\mu_n(\tau) = \langle (r_n(t) - r_n(t+\tau))^2 \rangle^{0.5}$; as the time scale τ we take 96 ps, which is much smaller than τ_{rot}.

Figure 9a shows the number of atoms that satisfy $\mu < \mu_n(96\text{ ps}) < \mu + d\mu$ in crystalline phase (blue), in an isotropic melt region far from the growing lamellae (red), and in the whole system (black). The crystalline atoms are generally seen to be less mobile compared with those in the melt, but they have a wider spectrum of mobility. In search for molecular origins of the wider spectrum of mobility in crystals, we here divide atoms according to their mobility into three types: low mobility type L with $\mu_n < 1$, high mobility type H with $\mu_n > 2$, and the intermediate mobility type M with $1 < \mu_n < 2$ (Figure 9a). In Figure 9b, we picked up all chains comprising the crystal and displayed their conformations with different colors according to the mobility of atoms, L (blue), M (green), and H (red); for ease of drawing only chains whose crystalline stems are located within the $y-z$ slab of thickness 2.5σ are shown. All atoms within each crystal stem have similar mobility (same color), which is a natural consequence of cooperative translation of the atoms. We notice that many of the amorphous segments (folds and cilia) also have similar mobility as those of the connected crystalline stems, which shows that the motions of crystalline stems and connected cilia or folds are strongly correlated. Also marked is that many of the crystalline stems linked to longer cilia are highly mobile (red), while those connected by tight folds seems to be severely restricted in motion (blue).

In order to confirm the expected correlation between the mobility of crystalline stems and conformations of the connected amorphous segments, we calculated for each chain j the averaged mobility $\bar{\mu}(j) = \sum_{i=1}^{100} \mu(i,j)/100$, where $\mu(i,j)$ is the mobility of the ith atom in the jth chain and the number of atoms forming folds or cilia $L_{folds+cilia}(j)$ for the jth chain. In Figure 9c are plotted the number of chains vs $L_{folds+cilia}$ for each $\bar{\mu}$ class: low mobility chains $\bar{\mu} < 1$, medium mobility chains $1 < \bar{\mu} < 2$, and high mobility chains $2 < \bar{\mu}$. Chains with low mobility have a distribution of $L_{folds+cilia}$ peaked around 20 bonds, which corresponds to the once-folded conformations of type A (Figure 1c); remember that the average stem length is about 40 bonds. On the other hand, chains of intermediate and high mobility have distributions peaked around $L_{folds+cilia} = 20$ bonds and $L_{folds+cilia} = 60$ bonds; the latter peak evidently corresponds to the half-crystallized chains of type B conformations (Figure 1c). Thus, most of the low mobility chains are found to have chain-folded conformation, supporting the general impression obtained from Figure 9b.

We have thus seen the presence of active but heterogeneous diffusion in crystals within a hundred picoseconds. Now we examine chain diffusion in much longer time scales. Recent NMR investigations on ultrahigh-molecular-weight PE have shown direct evidence of large-scale interphase diffusion between the crystalline and the amorphous phases. Similar observations were also reported in long-chain *n*-alkanes.[33,34] Though there is a great gap in the time scale of observation between NMR experiments and MD simulations; we here examine chain diffusion at 300 K, within our reachable time scale, between the crystalline and the amorphous phases. We count the number of atoms that have traveled between different phases; $N_{XB}(\tau)$ or $N_{XM}(\tau)$ for example denotes the number of atoms that have moved from the crystalline (X) phase to the boundary (B) phase (folds and cilia) or to the melt (M) phase within the time period between $t = 19.2$ ns and $t = (19.2 + \tau)$ ns, where $t = 19.2$ ns is selected since the transient melting at 360 K is finished around 15 ns (inset of Figure 7). Thus, we have obtained matrices of data $\{\mathbf{T}(\tau)\}$ showing frequencies of atomic transfer within $\tau = 0.192$, 1.92, 9.6, 19.2, and 30.72 ns:

$$\mathbf{T}(\tau) = \begin{pmatrix} N_{XX} & N_{XB} & N_{XM} \\ N_{BX} & N_{BB} & N_{BM} \\ N_{MX} & N_{MB} & N_{XM} \end{pmatrix} \tag{5}$$

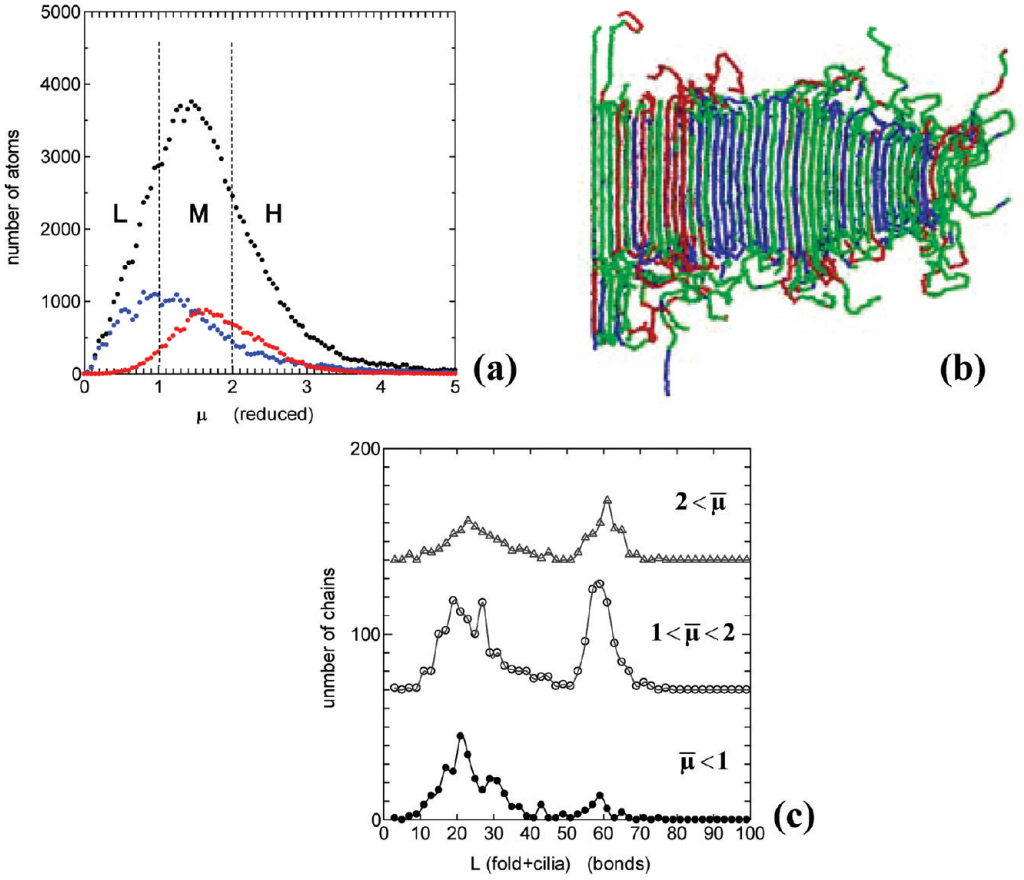

Figure 9. (a) Distributions of mobility (the average displacements of atoms within 96 ps) for atoms located in the crystalline region (blue circles), in the isotropic melt (red circles), and in the whole system (black circles). The mobility of atoms is divide into three regimes: low mobility regime (L) with $\mu < 1.0$, medium mobility regime (M) with $1.0 < \mu < 2.0$, and high mobility regime (H) with $2.0 < \mu$. (b) Snapshot of all chains forming the crystalline stems located at $|x| < 1.25\sigma$, where the atoms are plotted in different colors according to their mobility: L atoms in blue, M atoms in green, and H atoms in red. (c) Number of chains having a given length of surface atoms (folds plus cilia) for three types of chains of different mobility: L, M, and H.

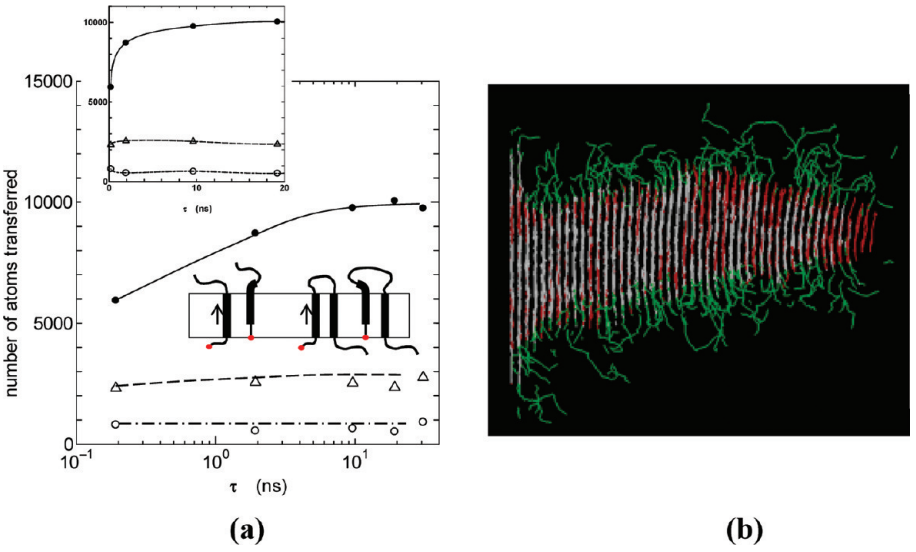

Figure 10. (a) Number of atoms that have shown transitions from the crystal to the boundary N_{XB} (●), from the boundary to the isotropic melt N_{BM} (Δ), and from the crystal to the melt N_{XM} (○), within given interval of time τ at 360 K. Inset is the same figure with the abscissa in linear scale. A possible molecular mechanism of the saturation in $N_{XB}(t)$ is also shown as a schematic picture, where chain ends are represented by red dots. (b) Typical snapshot of chains forming the chain-folded lamella at 360 K. The atoms are colored according to their relocation during 30.72 ns: from crystal to crystal (XX; white), from crystal to boundary or melt (XB; green), and from boundary or melt to crystal (B + M to X; red).

For any τ, the matrix **T** was found to be approximately symmetric ($N_{BX} \cong N_{XB}$, etc.), which indicates that the atomic transfers between the two phases are balanced. Of special interest are off-diagonal elements N_{XB}, N_{BM}, and N_{XM} vs τ (Figure 10a). The number of atoms that have moved from X to M or B to M is small and nearly constant, while the number of

atoms that have traveled from X to B is much larger and changes greatly with τ. It shows sharp initial increase but comes to saturate around 10 ns. Thus, interphase diffusion of chains within the present time scale of simulation is very active, but it is restricted probably due to pinning by the chain ends (see a schematic picture in Figure 10a). Now let us remember that the average length of cilia is about 15 bonds (Table 2). Possible average traverse of chains until the chains are pinned at the crystal surface is about 15 bonds (inset in Figure 10a). Since the number of the crystalline stems in the system is around 800 or slightly more (Table 2), the maximum number of transported atoms would be around 10^4 when we adopt the chain-end pinning mechanism. The limiting value of N_{XB} in Figure 10a is thus consistent with the chain-end pinning.

Figure 10b shows atoms immigrated, within 30.72 ns at 360 K, from X to X (white), from X to B or X to M (green), and from B to X or M to X (red); for ease of viewing we showed only atoms within the $y-z$ slab of thickens 4σ parallel to the crystalline chain axis. It is clearly noticed that considerable numbers of atoms are moving into the crystalline region (red), while about the same number of atoms are moving out of crystal into the boundary region (green).

4. Conclusions and Comments

In this paper we investigated the molecular process of melting in the chain-folded lamellae. We observed two types of melting with distinct molecular mechanism: reversible melting that takes place at the fold surface and irreversible melting at the growth front.

The fold-surface melting is nearly reversible if the temperature cycle is small and well below T_m, and it gives increasingly thinner lamellae at higher temperatures. It was found that the surface melting/recrystallization is not a process of simple release/recovery of the crystalline order at the fold surface, but active chain diffusion within the crystal is an essential prerequisite at least in our short polyethylene-like polymer.

The rate of the irreversible melting at the growth front, on the other hand, was found much slower and showed peculiar dependence on the degree of superheating. It would be interesting to consider that the accelerated melting at larger superheating would be in part due to progressively thinner lamellae as a consequence of larger surface melting. The molecular process of melting at the growth front involves the shortening of crystalline stems, detachment of whole chains, and final merging into the isotropic melt phase.

We also found that the mobility of chains in crystals have a rather wide spectrum. Many of the crystalline stems are less mobile than chains in the melt, but some stems connected to longer cilia or looser folds have unexpectedly large mobility. Such large dynamic heterogeneity in crystals was found to be closely correlated to the chain conformations at the fold surface.

Large diffusion of chains in the crystal was confirmed to yield frequent exchanges of constituent atoms between different phases: crystalline phase, surface amorphous phase, and the isotropic melt phase. Especially interesting was the segment transfer between the crystal and the surface amorphous layers. A considerable amount of segments moving between the crystalline and boundary/melt phases confirmed the dynamic aspect of the crystalline polymer.

Our present system consisted of short polyethylene-like polymers of uniform length just like long *n*-alkanes. Long *n*-alkanes usually take highly crystallized integer-fold structures.[39] However, it was recently reported that at the very beginning of crystallization under large supercooling, the crystallinity is rather small (around 50%) and the crystals are composed of both integer-folded chains and "half-crystallized" chains with long cilia and that the defective crystals reorganizes into much ordered ones after sufficient time of annealing.[40] Our simulated lamellae were grown at 340 K, the supercooling of about 40 K, within a hundred nanoseconds. Therefore, we may be studying the early stage of crystallization probably into a metastable crystalline state of long *n*-alkanes in highly supercooled conditions. Indeed, the simulated structures correspond well to those observed in long *n*-alkanes at the early stage of crystallization. In usual high-molecular-weight polymers, the dynamic heterogeneity must be much smaller, but similar structural heterogeneity at the fold surfaces will be present to some degree, causing similar dynamics heterogeneity in the crystals.

Our series of MD simulations including the present work cover time ranges of several hundreds of nanoseconds at the longest which are undoubtedly much shorter compared with experiments, even though the very early stage of crystallization of *n*-alkanes can be much faster than those in usual polymers. We must keep it in mind that the crystallization into the metastable states can be quantitatively different from usual crystallization. Indeed, the crystallinity attained in our simulation was only 50% in spite of experimental observations of highly crystalline states obtained in usual crystallization conditions. Therefore, various characteristic time constants reported in this work must not be taken as they are. In many cases, exact quantitative predictions are beyond the reach of our present simulations. Nevertheless, I believe the simulation methods can clarify and predict many essential features of crystallization in systems of long intertwined polymer molecules.

Acknowledgment. The present work was supported by the Grant-in-Aid of Scientific Research (No. 20550190) and by the past Grant-in-Aid of Scientific Research (No. 12127206) on Priority Area "Mechanism of Polymer Crystallization", both from the Ministry of Education, Science, and Culture, Japan.

References and Notes

(1) Wunderlich, B. *Macromolecular Physics*; Academic: New York , 1976; Vols. *1*−*3*.
(2) Mandelkern, L. *Crystallization of Polymers*; Cambridge University Press: Edinburgh, 2002; Vols. *1* and *2*.
(3) Hoffman, J. D.; Miller, R. L. *Polymer* **1997**, *38*, 3151.
(4) Allegra, G.; Famulari, A. *Polymer* **2009**, *50*, 1819.
(5) Armistead, K.; Goldbeck-Wood, G. *Adv. Polym. Sci.* **1992**, *100*, 219.
(6) Sommer, J.-U.; Reiter, G. *Polymer Crystallization*; Springer: Berlin, 2003.
(7) Allegra, G. *Interphases and Mesophase in Polymer Crystallization*; Adv. Polym. Sci.; Springer: Berlin, 2005; Vols. *180*, *181*, and *191*.
(8) Luo, C.; Sommer, J.-U. *Phys. Rev. Lett.* **2009**, *102*, 147801.
(9) Yamamoto, T. *J. Chem. Phys.* **2010**, *133*, 034904.
(10) Hu, W.; Thurn-Albrecht, T.; Strobl, G. *Macromolecules* **1999**, *32*, 7548.
(11) Goderis, B.; Reynaers, H.; Scherrenberg, R.; Mathod, V. B. F.; Koch, M. H. J. *Macromolecules* **2001**, *34*, 1779.
(12) Toda, A.; Hikosaka, M.; Yamada, K. *Polymer* **2002**, *43*, 1667.
(13) Lippits, D. R.; Rastogi, S.; Hoehne, G. W. *Phys. Rev. Lett.* **2006**, *96*, 218303.
(14) Thurn-Albrecht, T.; Strobl, G. *Macromolecules* **1995**, *28*, 5827.
(15) Zachmann, H. G. *Kolloid Z. Z. Polym.* **1969**, *231*, 504.
(16) Yamamoto, T. *Polymer* **2009**, *50*, 1975.
(17) Liu, C.; Muthukumar, M. *J. Chem. Phys.* **1998**, *109*, 2536.
(18) Meyer, H.; Mueller-Plathe, F. J. *Macromolecules* **2002**, *35*, 1241.
(19) Hu, W.; Frenkel, D.; Mathot, V. B. F. *Macromolecules* **2003**, *36*, 549.
(20) Gee, R. H.; Lacevic, N.; Fried, L. E. *Nature Mater.* **2006**, *5*, 39.
(21) Lacevic, N.; Gee, R. H.; Fried, L. E. *J. Chem. Phys.* **2008**, *128*, 014903.
(22) Yamamoto, T. *Adv. Polym. Sci.* **2005**, *191*, 37.
(23) Yamamoto, T. *J. Chem. Phys.* **2008**, *129*, 184903.
(24) Chen, C. M.; Higgs, P. G. *J. Chem. Phys.* **1998**, *108*, 4305.
(25) Doye, J. P.; Frenkel, D. *J. Chem. Phys.* **1998**, *109*, 10033.

(26) Waheed, N.; Lavine, M. S.; Rutledge, G. *J. Chem. Phys.* **2002**, *116*, 2301.
(27) Hu, W.; Frenkel, D.; Mathot, V. B. F. *Macromolecules* **2002**, *35*, 7172.
(28) Ma, Y.; Qi, B.; Ren, Y.; Ungar, G.; Hobbs, J. K.; Hu, W. *J. Phys. Chem. B* **2009**, *113*, 13485.
(29) Yamamoto, T.; Sawada, K. *J. Chem. Phys.* **2005**, *123*, 234906.
(30) Romanos, N. A.; Theodorou, D. N. *Macromolecules* **2010**, *43*, 5455.
(31) Steele, W. A. *Surf. Sci.* **1973**, *36*, 317.
(32) Schmidt-Rohr, K.; Spiess, H. W. *Macromolecules* **1991**, *24*, 5288.
(33) Klein, P. G.; Driver, M. A. N. *Macromolecules* **2002**, *35*, 6598.
(34) Grasso, G.; Titman, J. J. *Macromolecules* **2009**, *42*, 4175.
(35) Yao, Y.-F.; Graf, R.; Spiess, H. W.; Rastogi, S. *Macromolecules* **2008**, *41*, 2514.
(36) Yao, Y.-F.; Graf, R.; Spiess, H. W.; Lippits, D. R.; Rastogi, S. *Phys. Rev. E* **2007**, *76*, 060801.
(37) Welch, P.; Muthukumar, M. *Phys. Rev. Lett.* **2001**, *21*, 218302.
(38) Yamamoto, T. *J. Chem. Phys.* **1997**, *107*, 2653.
(39) Ungar, G.; Zeng, X. *Chem. Rev.* **2001**, *101*, 4157.
(40) Ungar, G.; Zeng, X.; Brooke, G. M.; Mohammed, S. *Macromolecules* **1998**, *31*, 1875.